Acta Pharmaceutica Sinica B 2025;15(7):3646−3662

Chinese Pharmaceutical Association
Institute of Materia Medica, Chinese Academy of Medical Sciences

Acta Pharmaceutica Sinica B

www.elsevier.com/locate/apsb
www.sciencedirect.com

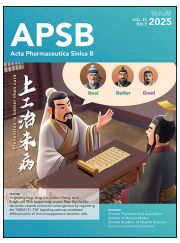

ORIGINAL ARTICLE

Discovery of *Yersinia* LcrV as a novel biased agonist of formyl peptide receptor 1 to bi-directionally modulate intracellular kinases in triple-negative breast cancer

Yunjun Ge[a,*], Huiwen Guan[a], Ting Li[c,d], Jie Wang[a], Liang Ying[a], Shuhui Guo[e], Jinjian Lu[c,d], Richard D. Ye[b,*], Guosheng Wu[a,*]

[a]*Department of Basic Medical Science, Wuxi School of Medicine, Jiangnan University, Wuxi, Jiangsu 214122, China; MoE Medical Basic Research Innovation Center for Gut Microbiota and Chronic Diseases, School of Medicine, Wuxi 214122, China*
[b]*Kobilka Institute of Innovative Drug Discovery, School of Medicine, the Chinese University of Hong Kong, Shenzhen 518172, China*
[c]*State Key Laboratory for Quality Research in Chinese Medicine, Institute of Chinese Medical Sciences, University of Macau, Macau SAR 999078, China*
[d]*MoE Frontiers Science Center for Precision Oncology, University of Macau, Macau SAR 999078, China*
[e]*Shenzhen Institute of Advanced Technology, Chinese Academy of Sciences, Shenzhen 518172, China*

Received 17 June 2024; received in revised form 27 March 2025; accepted 2 April 2025

KEY WORDS

G protein-coupled receptor;
Yersinia LcrV;
Biased agonist;
Formyl peptide receptor 1;
G protein;
Conformational change;
Signaling pathway;
Therapeutic strategy

Abstract G protein-coupled receptors (GPCRs) are significant drug targets, but their potential in cancer therapy remains underexplored. Conventional GPCR agonists or antagonists have shown limited effectiveness in cancer treatment, necessitating new GPCR-targeting strategies for more effective therapies. This study discovers that *Yersinia pestis* LcrV, a crucial linker protein for plague infection, acts as a biased agonist of a GPCR, the formyl peptide receptor 1 (FPR1). The LcrV protein induces unique conformational changes in FPR1, resulting in G proteins being activated in a distinctive state without subunit dissociation. This leads to a biased signaling profile characterized by cyclic adenosine monophosphate (cAMP) responses and β-arrestin2 recruitment, but not calcium mobilization. In FPR1-expressing triple-negative breast cancer (TNBC) cells, LcrV bi-directionally modulates intracellular signaling pathways, downregulating extracellular signal-regulated kinases (ERK1/2) and Akt pathways

*Corresponding authors.
E-mail addresses: 8202209002@jiangnan.edu.cn (Yunjun Ge), richardye@cuhk.edu.cn (Richard D. Ye), 8878700009@jiangnan.edu.cn (Guosheng Wu).

Peer review under the responsibility of Chinese Pharmaceutical Association and Institute of Materia Medica, Chinese Academy of Medical Sciences.

https://doi.org/10.1016/j.apsb.2025.04.030

while upregulating Jun N-terminal kinase (JNK) and p38 pathways. This dual modulation results in cell cycle arrest and the inhibition of TNBC cell proliferation. In TNBC xenograft mouse models, long-term LcrV treatment inhibits tumor growth more effectively than a conventional FPR1 antagonist. Additionally, LcrV treatment reprograms tumor cells by reducing stemness-associated proteins OCT4 and c-MYC. Our findings highlight the potential of biased GPCR agonists as a novel GPCR-targeting strategy for cancer treatment.

1. Introduction

GPCRs stand as the most efficacious drug targets in the therapeutic landscape of human diseases[1]. It is widely recognized that these receptors orchestrate essential growth signals that are pivotal to the proliferation of various cancer types, including breast cancer[2]. Traditional GPCR-targeted therapies aim at the development of conventional types of GPCR ligands, the agonists and antagonists, which have demonstrated modest success in cancer treatment[3]. As pharmacological research progressed, it was found that GPCR-targeted therapies could extend beyond conventional ligands to include more sophisticated variants, such as biased agonists or antagonists[4]. These biased ligands possess the unique ability to selectively modulate specific GPCR-mediated signaling pathways, in contrast to traditional ligands that activate or suppress all GPCR signaling without bias[5]. By activating desired signaling pathways while circumventing those that induce adverse effects, biased ligands present therapeutic advantages over their traditional counterparts.

Canonical GPCR signaling involves the dissociation of the Gα and G$\beta\gamma$ subunits upon receptor activation, followed by the association of the G$\beta\gamma$ subunit with G protein-coupled receptor kinases (GRKs)[3,6]. Fully activated G proteins initiate intracellular cAMP responses and calcium mobilization. Additionally, β-arrestin proteins are usually recruited to the activated receptor, followed by receptor internalization. G proteins and β-arrestins play central roles in activating the signaling pathways of the mitogen-activated protein kinase (MAPK) and phosphatidylinositol-3-kinase (PI3K)/Akt through intricate signaling cascades[7–9]. These pathways are pivotal for cell proliferation and differentiation, particularly in cancer cells[7,10]. It is worth noting that distinct MAPK and PI3K/Akt signaling pathways can offer varying, sometimes contradictory, signals for tumor growth. More specifically, the activation of ERK1/2 and PI3K/Akt pathways tends to promote tumor growth, while the activation of other MAPK pathways, such as p38 and JNK, may inhibit it under certain conditions[11–14].

Formyl peptide receptors (FPRs), including FPR1, FPR2, and FPR3 in humans, form a subclass of GPCRs aberrantly expressed in various cancers, including breast cancer[15,16]. These receptors mediate cell proliferation signals in breast cancer, particularly in the TNBC subtype, which lacks the typical growth-promoting receptors, estrogen receptor, progesterone receptor, and human epidermal growth factor receptor 2 (HER2)[17]. The use of FPR1 antagonists has been proposed as a therapeutic strategy for TNBC[18,19]. FPRs can be activated by pathogen- or damage-associated formyl peptides and other ligands with diverse chemical properties[20,21]. Universal ligands like annexin A1 and mitochondrial formylated peptides can activate FPR1 and trigger various intracellular signaling pathways, primarily through the inhibitory Gα (Gαi) and G$\beta\gamma$ complex[22]. FPR ligands do not uniformly activate downstream signaling pathways. Reports have shown that FPR2 can exert two opposing functions through the mechanism of biased signaling[23,24].

Yersinia pestis, the bacterium responsible for causing the plague, disrupts human immune cells, proliferates in the bloodstream, and is transmitted to new hosts through flea bites[25]. The bacterium employs a type III secretion system to inject virulence proteins into human immune cells, allowing it to evade host immune responses[26]. The LcrV protein is the needle cap protein within the bacterium's type III secretion system[27]. The LcrV protein was identified as a binding protein of FPR1 and their interactions were crucial for plague infection[28]. The LcrV protein alone was not able to stimulate the migration of FPR1-expressing cells, thus lacking the classical properties of FPR1 agonists[28]. However, the LcrV protein was able to stimulate the release of interleukin-10 protein from FPR1-expressing cells[29,30]. Furthermore, the LcrV protein could inhibit lipopolysaccharide-stimulated tumor necrosis factor-alpha secretion from FPR1-expressing cells[30]. Although there is no direct evidence that these actions are mediated by FPR1, it remains possible that LcrV functions as a biased ligand of FPR1, selectively inducing signaling pathways to provoke specific cellular responses.

In this study, we demonstrated that the *Yersinia pestis* LcrV protein is a novel biased agonist of FPR1. The LcrV protein activates FPR1 to a specific conformational state, leading to the unconventional activation of the G protein complex and β-arrestin2 with a biased signaling repertoire. The peculiar activation states of the signaling cascade lead to bi-directional modulation of MAPK and PI3K/Akt signaling pathways in TNBC cells, resulting in enhanced anti-tumor effects *in vivo* compared to a conventional FPR1 antagonist. Our findings highlight the potential of using biased ligands as a novel strategy for targeted cancer therapy to achieve improved anti-tumor outcomes.

2. Materials and methods

2.1. Cell culture

HEK293T and RBL-2H3 cells were purchased from the American Type Culture Collection. The cell lines, MDA-MB-231, 4T1, and MDA-MB-468, were obtained from the National Collection of Authenticated Cell Cultures (Shanghai, China). A stable FPR1-transfected RBL-2H3 cell line (FPR1-RBL) was created through G418 selection for two months following transient transfection. HEK293T, MDA-MB-231, and MDA-MB-468 cells were cultured in Gibco BASIC DMEM (Thermo Fisher Scientific, Waltham,

MA, USA) supplemented with 10% Hyclone Fetal Bovine Serum (FBS; Cytiva, Marlborough, MA, USA) at 37 °C in a 5% CO_2 atmosphere. The 4T1 cells were cultured in Gibco RPMI 1640 Medium supplemented with 10% FBS. FPR1-RBL cells were cultured under similar conditions with 20% FBS and 0.2 mg/mL G418. All related experiments were conducted with the cell lines within 3−20 passages from the original stocks.

2.2. *LcrV expression and purification*

The *Yersinia pestis LcrV* gene (GenBank: KF682423.1) was cloned into the pET28a(+) vector. The plasmids were then transfected into BL21(DE3) *E. coli*, and protein expression was induced by adding 500 nmol/L isopropyl β-D-thiogalactoside (IPTG) for 8 h. The bacteria were lysed and sonicated in a hypertonic buffer containing 500 mmol/L NaCl, 100 μg/mL phenylmethylsulfonyl fluoride, and 20 mmol/L HEPES/NaOH at pH 7.5. The lysate, containing His-tagged LcrV proteins, was incubated with Ni-NTA resin at 4 °C for 1 h. The LcrV-bound Ni-NTA resin was collected by centrifugation, and the LcrV proteins were eluted using a buffer with 250 mmol/L imidazole, 500 mmol/L NaCl, and 20 mmol/L HEPES/NaOH at pH 7.5. The LcrV proteins were further purified using size exclusion chromatography with a Superdex 200 Increase 10/300 GL column on the AKTA pure chromatography system (Cytiva). The purified LcrV proteins were collected in a working solution of 100 mmol/L NaCl and 20 mmol/L HEPES/NaOH at pH 7.5, aliquoted, and stored at −80 °C. The purity was greater than 95% as determined by reducing SDS-PAGE and size exclusion chromatography.

2.3. *FPR1 conformation analyses*

Conformational analyses were based on a fluorescein arsenical hairpin binder (FlAsH)-based bioluminescence resonance energy transfer (BRET) technology as previously reported[31]. In brief, a plasmid was constructed to express a modified FPR1 with a CCPGCC motif in the third intracellular loop and a NanoLuc gene at the C-terminus. The biosensor was expressed in HEK293T cells and labeled with 500 nmol/L TC-FlAsH dye (Thermo Fisher Scientific, T34561) for 1 h. The cells were collected in HBSS buffer with 20 mmol/L HEPES at a density of 1×10^6 cells/mL and incubated with 5 μmol/L coelenterazine h (Yeasen Biotechnology, Shanghai, China; 40906 ES) for 5 min in a white 96-well plate. Different concentrations of fMLF (Sigma, Livonia, MI, USA; F3506) or LcrV were added to the cells and the plate was loaded on the FlexStation 3 Microplate Reader (Molecular Devices, San Jose, CA, USA) immediately. Fluorescence intensities at wavelengths of 515 nm and 460 nm were measured for 5 min. BRET signals were calculated as ratios of the intensities (Em 515 nm/Em 460 nm) subtracted by the bleed-through ratio of NanoLuc. Averages of the BRET signals in each well were recorded as the responses.

2.4. *G protein subunit dissociation*

The dissociation of the G$\alpha\beta\gamma$ subunit was analyzed using NanoBiT technology as previously described[32,33]. A plasmid was engineered to express a modified Gαi1 protein with the large fragment of NanoLuc luciferase (LgBiT) inserted into its helical domain, specifically between the αA and αB helices (between residues 91 and 92) of Gαi1. Another plasmid was designed to express a modified Gγ2 protein with the small fragment of NanoLuc (SmBiT) at its N-terminal. These two plasmids, along with plasmids coding for FPR1 and Gβ1, were co-transfected into HEK293T cells. One day post-transfection, the cells were collected in white 96-well plates and incubated with 10 μmol/L coelenterazine h for 2 h. Baseline luminescence signals in the plate wells were measured for 5 min using the EnVision Multimode Plate Reader (PerkinElmer, Waltham, MA, USA). Varying concentrations of fMLF or LcrV were then added to the wells. Following the treatment, luminescence signals were re-measured for additional 15 min. The average luminescence intensities measured from 10 to 15 min post-stimulation were divided by the averaged baseline intensities to obtain relative luminescence intensities. Concentration-dependent response curves were plotted using GraphPad Prism software.

For Gαq activation, a plasmid was constructed to encode a modified Gαq protein with LgBiT inserted between residues 97 and 98 of Gαq, with another plasmid coding for RIC8A. These two proteins were co-expressed together with FPR1, Gβ1, and SmBiT-tagged Gγ2 in HEK293T cells. The dissociation assays were conducted in a manner similar to that described above. Luminescence signals were detected using the EnSight Plate Reader (PerkinElmer), as the EnVision reader was unavailable during this assay.

2.5. *G$\beta\gamma$-GRK association*

A bimolecular fluorescence complementation (BiFC)-based BRET assay was applied, and relevant plasmids were constructed as previously described[34]. The yellow fluorescent protein (YFP) fragment (155−238) was fused to the N-terminal of the G protein β1 subunit, while the YFP fragment (1−154) was fused to the N-terminal of Gγ2, connected by a flexible linker (GSGGSGGSGGSG). NanoLuc luciferase was tagged at the N-terminus with a membrane anchor (MGCIKSKGKDS) and fused to the GRK3 fragment (GRK3ct; the C-terminal region of GRK3), connected by two flexible linkers. The tagged G$\beta\gamma$ and GRK3ct were co-expressed with FPR1 and Gαi1 in HEK293T cells for 24 h. The cells were collected in white 96-well plates and incubated with 10 μmol/L coelenterazine h for 5 min. Fluorescence emission signals at 460 nm and 535 nm were detected using the EnVision Plate Reader. The BRET signals were calculated as the ratio of the intensities of the two emission channels (Em 535 nm/Em 460 nm). LcrV, fMLF, or PBS were added during the machine reading, and real-time signals before and after ligand stimulation were recorded for 2−5 min. Data were fitted to a plateau followed by a one-phase decay equation in GraphPad Prism using the least squares fit method.

2.6. *Calcium mobilization and cAMP measurement*

For calcium mobilization, FPR1-RBL-2H3 cells or MDA-MB-231 cells were seeded into 96-well clear-bottom black plates and incubated with Calcium 5 dye (Molecular Devices, R8186) in HBSS buffer supplemented with 20 mmol/L HEPES for 1 h. The plates were then loaded into the FlexStation 3 Microplate Reader (Molecular Devices), and varying concentrations of FPR1 ligands were added during the recording. Fluorescence signals were measured at an emission wavelength of 535 nm with an excitation wavelength of 485 nm. Calcium responses were calculated as the difference between the maximum and minimum fluorescence intensities, expressed in Relative Fluorescence Units (RFU).

For cAMP measurement, a fluorescence resonance energy transfer (FRET) biosensor was created based on mTurquoise2-Epac SH187-cp73venus-cp73venus as described before[33]. The cAMP biosensor and FPR1 were co-expressed in HEK293T cells for 24 h. The cells were collected in 96-well black plates, and incubated with FPR1 ligands and 5 μmol/L forskolin in stimulation buffer (HBSS plus 5 mmol/L HEPES, 0.1% BSA (*w*/*v*), and 0.5 mmol/L isobutylmethylxanthine) for 30 min. After incubation, the plates were loaded on the FlexStation 3 Microplate Reader (Molecular Devices) and fluorescence emission intensities at 485 nm and 535 nm upon excitation at 430 nm were recorded. The reduction in normalized FRET ratio of fluorescence emission at 485 nm divided by emission at 535 nm reflected the cAMP responses.

2.7. β-Arrestin2 recruitment

Plasmids were constructed to express FPR1 with NanoLuc fused at the C-terminus and C-terminal GFP-tagged β-arrestin2. These tagged proteins were co-transfected into HEK293T cells. One day post-transfection, the cells were harvested in HBSS buffer supplemented with 20 mmol/L HEPES at a density of 1×10^5 cells/100 μL. Following a 10-min incubation with 5 μmol/L coelenterazine h, varying concentrations of fMLF or LcrV were used to stimulate β-arrestin2 recruitment. The assays were performed in a white 96-well plate, and fluorescence intensity was measured using the Envision Plate Reader (PerkinElmer). Fluorescence intensities at 515 nm and 460 nm wavelengths were recorded over 30 min post-treatment. BRET signals were calculated as the ratios of these intensities (Em 515 nm/Em 460 nm) after subtracting the NanoLuc bleed-through ratio. The maximal BRET signal from each well was recorded as the response.

2.8. FPR1 internalization

FPR1-RBL cells were collected at a density of 1×10^6 cells/mL in HBSS buffer with 20 mmol/L HEPES. The cells were treated with LcrV, fMLF, or PBS for 1 h in a cell incubator. After removing the ligands, the cells were stained with a fluorescent FPR1-specific antibody (BD, Franklin Lakes, NJ, USA; 565623) on ice for 30 min. Non-specific antibody binding was removed by washing with PBS. Cell fluorescence was detected using the BD Accuri C6 Flow Cytometer (Becton, Dickinson and Company), with the fluorescence intensities reflecting the cell surface protein levels of FPR1 after ligand treatment.

For confocal microscopy, mCherry-tagged FPR1 was expressed in HEK293T cells. The cells were stimulated with ligands for 20 min, fixed with 4% paraformaldehyde, and permeabilized with 0.1% Triton X-100. Rab5 was stained as an endosome marker using a fluorescent antibody (Supporting Information Table S1), and the cell nuclei were stained with Hoechst 33342. FPR1 internalization was analyzed using the TCS SP8 confocal microscope (Leica Microsystems Inc., Wetzlar, Germany). Images from different channels were captured using a 63 × oil immersion lens and merged using the microscope software.

2.9. Western blotting analyses

Cells of FPR1-RBL-2H3 or MDA-MB-231 were cultured in 12-well plates and starved in serum-free DMEM for 4 h. The cells were then treated with 2 μmol/L LcrV or 1 μmol/L fMLF for varying durations. Protein samples were extracted using 95 μL of cell lysis buffer containing protease inhibitors per well. After denaturation, the proteins were separated using SDS-PAGE gels and transferred to PVDF membranes. Specific primary antibodies and HRP-linked secondary antibodies were used to detect total and phosphorylated MAPK and Akt proteins according to the manufacturer's instructions. Blot images were captured using the ChemiDoc Imaging Systems (Bio-Rad Laboratories, Hercules, CA, USA), and protein levels were quantified using Bio-Rad Image Lab software. The average protein levels from multiple experiments were normalized for statistical analysis.

For G protein inhibition, pertussis toxin (PTX) was obtained from Absin Bioscience (Shanghai, China; abs42024900). The inhibitory activity of this agent was validated through a preliminary experiment with cAMP response (data not shown). MDA-MB-231 cells were treated with PTX (100 ng/mL) for at least 6 h before LcrV stimulation. For β-arrestin2 knockdown, three siRNAs were designed and synthesized by Jiangsu Genecefe Biotechnology (Wuxi, China). The sequences are as follows: siRNA-1: 5′-CCACCAAGACCGUCAAGAA-3′, siRNA-2: 5′-GGCUCAACUCGAACAAGAU-3′, and siRNA-3: 5′-CCUACAGGGUCAAGGUGAA-3′. These siRNAs were utilized to knock down β-arrestin2 expression in MDA-MB-231 cells. The siRNAs were transfected into the cells for three days, after which β-arrestin2 protein levels were detected using a specific antibody in immunoblotting, as described above.

Tumor samples weighing 20 mg were lysed in 200 μL of lysis buffer. The expression of OCT4, c-MYC, SOX2, β-catenin, and β-actin was detected using specific antibodies. Immunoblotting analyses were performed following the same procedures as described above. Information about all the related antibodies was listed in Table S1.

2.10. Bioinformatic analyses

The significant associations of FPR1 between tumor and adjacent normal tissues in multiple cancer types in TCGA were analyzed using the Gene_DE module in TIMER2.0 (the Tumor Immune Estimation Resource, Version 2.0, http://timer.cistrome.org/) for Cancer Exploration[35]. The survival plots of FPR1 expression with overall survival and relapse-free survival were generated based on the analysis of 104 breast cancer biopsies (GEO: GEO42568) using BEST (Biomarker Exploration for Solid Tumors, version 1.1, https://rookieutopia.com/)[36] with Group cutoff method of the median. The log-rank *P*-value was analyzed using the Kaplan−Meier method. PAM50 analysis using gene expression data from 266 breast cancers, quantified by whole-genome DNA microarrays (GEO: GSE21653), was then performed to intrinsically subtype and calculate the contribution of FPR1 expression (z-score) to archival tissue.

2.11. Cancer cell functional assays

Cells were incubated in a 6-well plate and treated with FPR1 ligands for 48 h. The cells were then collected and fixed in 75% ethanol at 4 °C for 24 h. After fixation, the cells were washed with cold PBS, digested with 0.5 μg/mL RNase A, and stained with 50 μg/mL propidium iodide (PI) at 37 °C for 30 min in the dark. DNA levels were measured using the BD LSRFortessa Cell Analyzer, and cell cycle analysis was performed using BD FlowJo v10 software.

For cell proliferation assays, cells were seeded in 96-well plates and incubated with various concentrations of FPR1 ligands for 24 h.

The cells were then treated with 5 mg/mL MTT, and the resulting formazan was solubilized with dimethyl sulfoxide for 10 min. Absorbance at 490 nm for each well was recorded using the Synergy H4 Microplate Reader (BioTek Instruments, Winooski, VT, USA).

For limited dilution analysis, MDA-MB-231 cells were treated with 2 μmol/L LcrV or PBS (control) for one week. The cells were prepared as single-cell suspensions and serially diluted to different doses. For each dose, the cells were seeded into 24 or 96 wells of 96-well plates. Three weeks later, wells containing spheres were counted, and the number of positive wells was used to calculate the cancer cell initiating frequency and significance with the ELDA software[37].

2.12. *In vivo xenograft mouse models*

Animal experiments were carried out with the approval of the Experimental Animal Care and Use Committee at Jiangnan University, in accordance with the World Medical Association (WMA) Statement on animal use in biomedical research, and adhering to the previously described criteria[38]. Female BALB/c nude or BALB/c mice, aged between 4 and 6 weeks, were procured from SPF Biotechnology Co., Ltd. (Beijing, China). MDA-MB-231 cells (3×10^6) were subcutaneously inoculated into the mammary fat pads of BALB/c nude mice. For the 4T1-xenografted mouse model, 5×10^5 cells were implanted into BALB/c mice. Approximately two weeks later, the mice were randomly allocated into three groups. Treatments were administered once every two days *via* intratumoral injections, utilizing either PBS, LcrV protein, or cyclosporine H. To evaluate anti-tumor effects, doses of 20 μL of LcrV (5 μmol/L) or cyclosporine H (20 μmol/L) for each mouse were employed. Tumor progression was tracked by measuring tumor dimensions in length (L) and width (W), with tumor volumes (TV) calculated according to Eq. (1):

$$\mathrm{TV} = 0.5 \times L \times W^2 \quad (1)$$

Additionally, the body weights of all mice were recorded throughout the treatment period. At the conclusion of the experiments, tumor specimens were collected for imaging and weight assessments. Histological analysis involving H&E staining was performed on liver and lung tissues from the mice, in accordance with previously outlined methods.

2.13. *Statistical analysis*

The data were analyzed using GraphPad Prism 5 software (GraphPad Inc., La Jolla, CA, USA). Results are presented as means ± standard error of mean (SEM) from at least three independent experiments. Unless otherwise indicated, differences between two groups were assessed using Student's t-test, with a P-value of <0.05 considered statistically significant. Differences among multiple groups were analyzed using one-way analysis of variance (ANOVA).

3. Results

3.1. *Yersinia pestis LcrV protein stimulated conformational changes of FPR1 receptor*

The previous study found that *Yersinia pestis* LcrV protein could bind to human FPR1 receptor, which was a crucial step in plague infection[28]. Although the LcrV protein did not stimulate FPR1-mediated chemotaxis as reported in the previous study, we were interested in understanding how LcrV affected the conformational state of FPR1 and the intracellular signaling mediated by this receptor. For this reason, *Yersinia pestis* LcrV protein was produced and purified for further analysis. The *Yersinia pestis LcrV* gene was cloned into the pET28(+) vector, and the LcrV protein was expressed in BL21(DE3) *E. coli* (Fig. 1A). The LcrV proteins were then harvested using Ni-affinity purification and further purified through size exclusion chromatography (Fig. 1B). The LcrV protein was confirmed by Western blotting analysis, with the purity (greater than 95%) determined by reducing SDS-PAGE and size exclusion chromatography (Fig. 1C and D).

To investigate LcrV influences on FPR1, an intramolecular BRET biosensor was created to analyze FPR1 conformational state. The biosensor was created with a CCPGCC motif inserted into the third intracellular loop of FPR1 and the Nanoluc protein tagged at the C terminus of the receptor (Fig. 1E). The changes in BRET signals were measured to reflect intramolecular interactions between the two labeled sites of FPR1 receptor (Fig. 1E). When applied to stimulate FPR1, the LcrV proteins at micromolar concentrations increased the BRET signals of the biosensor compared to the control treatment (Fig. 1F). This result revealed that the distance between the two labeled sites of the FPR1 biosensor decreased after LcrV stimulation, indicating that LcrV could stimulate conformational changes of FPR1. As a positive control, the conventional FPR1 agonist fMLF at nanomolar to micromolar concentrations stimulated conformational changes that decreased the BRET signals (Fig. 1F). These results indicated that LcrV could activate FPR1, but the resulting conformational states were different from those induced by the classical agonist fMLF.

3.2. *G protein heterotrimer was activated by LcrV without subunit dissociation*

To further investigate LcrV influences on FPR1-mediated signaling, the activation state of the canonical signaling mediator G protein complex, composed of Gα, Gβ, and Gγ subunits, was examined. Both Gαβγ subunit dissociation and Gβγ−GRK association are indicative of G protein activation[34]. Gαβγ subunit dissociation was measured using a NanoBiT complementation assay. Fragments of the Nanoluc protein were tagged to the Gα and Gβγ subunits, respectively (Fig. 2A). The dissociation of the G protein complex resulted in a decrease in the luminescence signals of the Nanoluc protein. The modified Gαβγ subunits were co-expressed with FPR1 in HEK293T cells and stimulated by LcrV or fMLF. In a Gαi-Gβγ dissociation assay, the full agonist fMLF induced a concentration-dependent decrease in the relative luminescence intensities, indicating the dissociation of the Gαi subunit from the Gβγ subunit (Fig. 2B). However, in contrast to the full agonist, LcrV did not stimulate the dissociation of the G protein heterotrimer at concentrations up to 10 μmol/L (Fig. 2B). Similarly, in a Gαq−Gβγ dissociation assay, LcrV did not stimulate the dissociation of Gαq from the G protein complex, whereas the agonist fMLF did (Supporting Information Fig. S1).

A YFP complementation-based BRET assay was created to detect Gβγ−GRK3 association as described previously[34]. In this assay, YFP fragments were labeled to Gβγ subunits and Nanoluc protein was labeled to the C-terminal fragment of GRK3 (GRK3ct) (Fig. 2C). The labeled Gαβγ subunits and GRK3ct were co-expressed with FPR1 in HEK293T cells and then

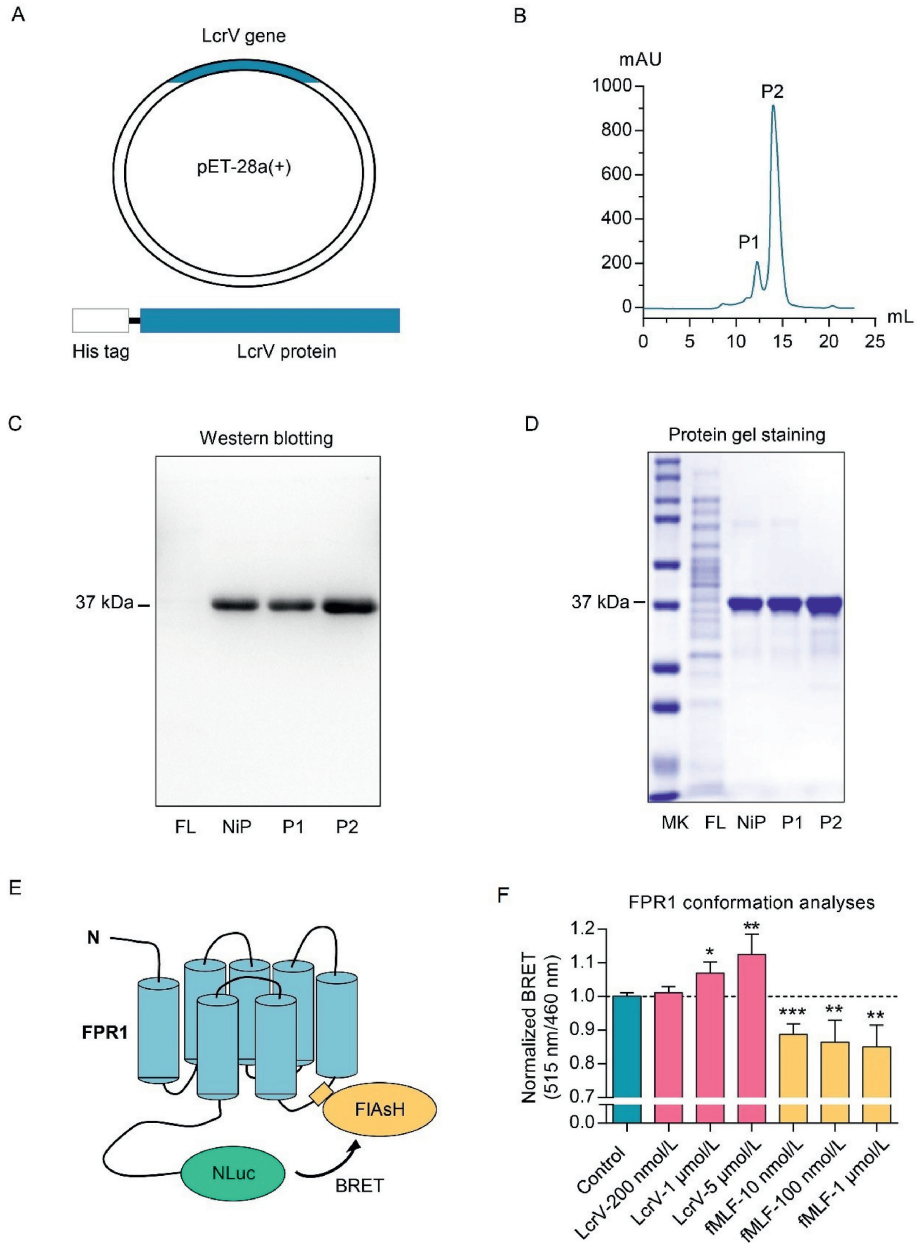

Figure 1 FPR1 conformational changes induced by the purified LcrV proteins. (A) Plasmid construct of His-tagged LcrV. (B) Size exclusion chromatography of LcrV proteins. A representative chromatogram is shown, and protein samples were collected at the indicated peaks (P1 and P2). (C) Western blot analysis of LcrV proteins. The proteins were analyzed using anti-His antibodies. FL denotes flowthrough samples of cell lysate during Ni-NTA purification. NiP denotes Ni-NTA purified proteins. P1 and P2 correspond to the peaks shown in (B). (D) Coomassie blue staining of LcrV proteins. Proteins were separated on an SDS-PAGE gel by electrophoresis and stained. MK denotes protein markers. (E) FlAsH-based BRET biosensor. The CCPGCC motif is shown in yellow. NLuc denotes the Nanoluc protein. FlAsH denotes the membrane-permeant fluorescent dye. (F) BRET analyses of FPR1 conformations. BRET signals were subtracted by NanoLuc crosstalk signal and normalized to the control. Data are presented as mean ± SEM ($n = 3$). *$P < 0.05$, **$P < 0.01$, and ***$P < 0.001$.

stimulated with fMLF, LcrV, or buffer as a control. It was observed that the full agonist fMLF could stimulate the increase of the BRET signals within 20 s, indicating the association of G$\beta\gamma$ with GRK3 (Fig. 2D). The LcrV protein also stimulated an obvious increase of the BRET signals, which was comparable to that of the full agonist fMLF, albeit with a weaker response (Fig. 2D). These findings indicate that LcrV is capable of inducing a specific activation state of the G protein complex without causing G protein subunit dissociation. This effect is likely due to the specific conformational state of FPR1 after LcrV stimulation as described above.

3.3. Biased signaling of FPR1 was stimulated by LcrV with receptor internalization

Stimulation of FPR1 and G protein activation usually leads to cAMP and calcium responses[39]. The cAMP response of FPR1−Gαi signaling was investigated using the Epac-based FRET

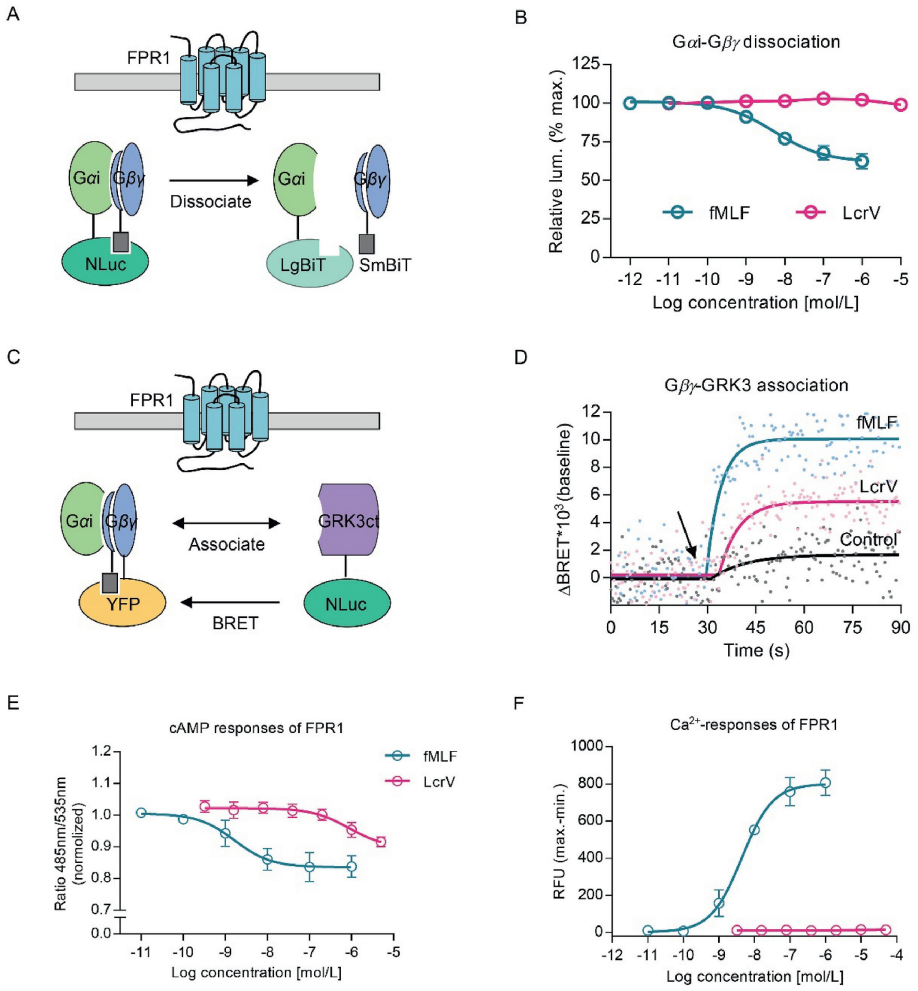

Figure 2 Activation of the G proteins and biased signaling of FPR1 following ligand stimulation. (A) NanoBiT-based G protein subunit dissociation assay. The large fragment of NanoLuc luciferase (LgBiT) is shown in green and the small fragment (SmBiT) is shown in gray. (B) Luminescence signals of the NanoBiT assay. The signals were shown by relative luminescence intensities (Relative Lum.), which were further calculated as percentages of the maximal relative intensity. No significance was found between the control and each LcrV treatment. (C) BiFc-based BRET assay for G$\beta\gamma$−GRK3 association. YFP fragments, shown in yellow or gray, were fused to Gβ and Gγ subunits, respectively. (D) Real-time detection of BRET signals. The cells were stimulated at the indicated time point as shown by the arrow. Real-time BRET signals were subtracted by average signals before stimulation to calculate ΔBRET. Representative curves fitted to a plateau followed by a one-phase decay equation from three independent experiments are shown. (E) Intracellular cAMP responses of FPR1. FPR1 was stimulated with the indicated concentrations of fMLF or LcrV for 30 min. FRET signals were normalized to the control buffer treatments. (F) Calcium responses of FPR1. FPR1 was stimulated as indicated in (E). RFU stands for relative fluorescence units. Data are presented as mean ± SEM from at least three independent experiments.

biosensor, as detailed in the Methods section. It was found that LcrV can reduce intracellular cAMP levels similarly to the full agonist fMLF in FPR1-transfected cells (Fig. 2E). LcrV induced a concentration-dependent cAMP response with an EC_{50} value of 0.9 μmol/L. Calcium response of FPR1 was assessed using the Calcium 5 dye in FPR1-stably transfected cells. In contrast to the cAMP responses, LcrV did not elicit a calcium response at concentrations up to 50 μmol/L, while the full agonist fMLF induced a concentration-dependent calcium response (Fig. 2F). These findings demonstrate that LcrV activates FPR1 and triggers biased signaling pathways. The bias towards the cAMP response, but not the calcium response, is likely caused by the specific activation state of the G protein complex downstream of FPR1.

In addition to G protein activation, the stimulation of FPR1 is frequently accompanied by the recruitment of β-arrestins, which play roles in regulating receptor internalization and downstream signaling. FPR1 and β-arrestin2 were tagged with NanoLuc and GFP, respectively, and their interaction was evaluated by monitoring changes in BRET signals. In cells expressing the modified FPR1 and β-arrestin2, LcrV was found to increase the BRET signals, similar to the effect of fMLF. This indicates the recruitment of β-arrestin2 to FPR1 (Fig. 3A). To investigate FPR1 internalization, cell surface FPR1 was labeled with fluorescent anti-FPR1 antibodies and analyzed by flow cytometry. Following LcrV treatment, the protein level of FPR1 at the cell surface decreased, consistent with β-arrestin recruitment (Fig. 3B). The

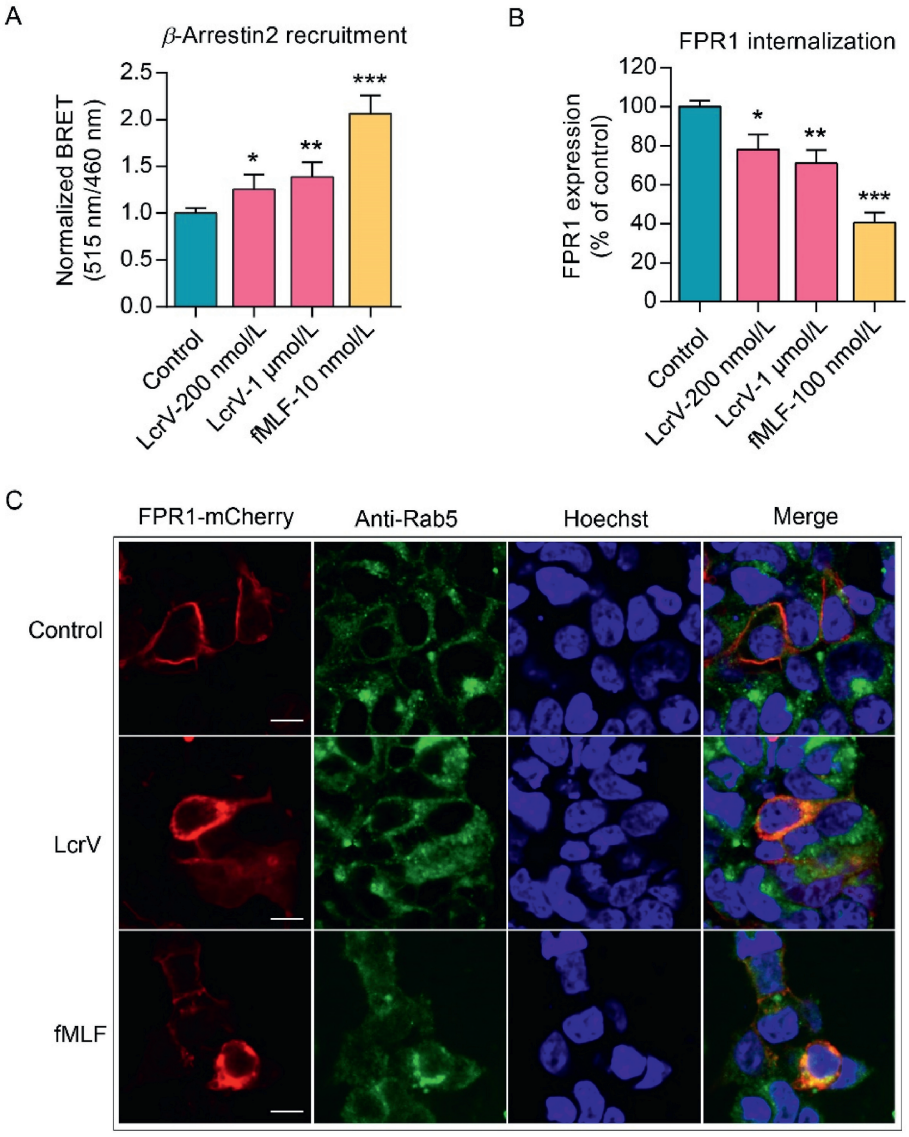

Figure 3 LcrV-induced β-arrestin2 recruitment and FPR1 internalization. (A) β-arrestin2 recruitment to FPR1. FPR1 was stimulated and BRET signals were detected as indicated. (B) Flow cytometry of FPR1 internalization. FPR1-expressing cells were stimulated as indicated. Cell surface receptors were analyzed with FPR1-specific fluorescent antibodies. Data are presented as mean ± SEM from at least three independent experiments. $^{*}P < 0.05$, $^{**}P < 0.01$, and $^{***}P < 0.001$. (C) Confocal microscopy of FPR1 internalization. The fluorescently labeled FPR1, displayed in red, was stimulated with 100 nmol/L fMLF or 1 μmol/L LcrV. Rab5 was stained with a fluorescent antibody and displayed in green. The cell nuclei were depicted in blue. Representative images from three independent experiments are presented. Scale bar = 10 μm.

internalization of FPR1 induced by LcrV was additionally confirmed through the microscopic examination of fluorescently labeled FPR1 in HEK293T cells (Fig. 3C).

3.4. LcrV bi-directionally modulated specific MAPK and PI3K/Akt signaling pathways

G protein and β-arrestins play central roles in regulating the MAPK and PI3K/Akt signaling pathways[3]. To investigate LcrV influences on these pathways, FPR1-expressing cells were stimulated with 2 μmol/L LcrV or 1 μmol/L fMLF, and phosphorylation levels of ERK1/2, JNK, p38, and Akt proteins were analyzed by Western blotting. The conventional agonist fMLF was found to stimulate time-dependent activation of both signaling pathways, as evidenced by elevated phosphorylation levels of ERK1/2, JNK, p38, and Akt proteins (Fig. 4A and Supporting Information Fig. S2A). As a biased FPR1 agonist, the LcrV protein stimulated partial activation of the MAPK signaling pathways, as evidenced by the elevated phosphorylation levels of JNK and p38 kinases (Fig. 4B and Fig. S2B). However, for ERK1/2 and Akt, the LcrV protein reduced rather than increased the phosphorylation levels of the kinases (Fig. 4B and Fig. S2B).

Quantification analyses further revealed that the biased FPR1 agonist LcrV stimulated a bi-directional modulation of the intracellular signaling pathways, while the full FPR1 agonist fMLF stimulated a unidirectional modulation of the pathways (Fig. 4C). This is likely caused by the unique activation state of the G protein heterotrimer upon LcrV stimulation of FPR1 (Fig. 2B and D). MAPK and PI3K/Akt signaling play pivotal roles in the proliferation of cancer cells, where FPR1 expression has been reported.

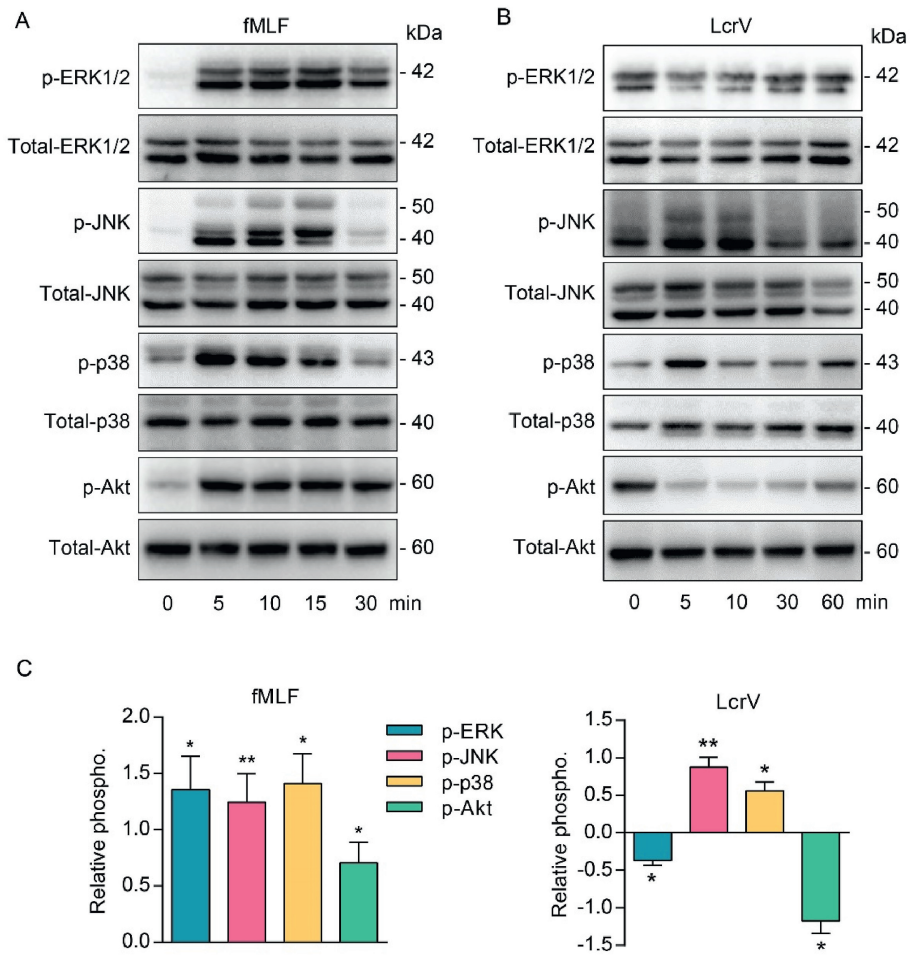

Figure 4 FPR1-mediated MAPK and PI3K/Akt signaling pathways. (A) Activation of MAPKs and Akt by fMLF. FPR1-RBL cells were stimulated with 1 μmol/L fMLF for the specified durations. Total and phosphorylated kinases were analyzed by Western blotting. Representative blots from at least three experiments are shown. (B) Stimulation of MAPKs and Akt by LcrV. FPR1 were stimulated with 2 μmol/L LcrV. Representative blots from at least three experiments are shown. (C) Quantification of phosphorylated protein levels. The densities of the blots from at least three independent experiments were measured, and the phosphorylation (phospho.) level relative to the total protein level was calculated. The maximum increase or decrease after stimulation was chosen, and the basal phosphorylation level was set to zero. Data are presented as mean ± SEM ($n = 3–4$). *$P < 0.05$, and **$P < 0.01$.

This prompted the speculation that the LcrV protein might be able to regulate tumor growth.

3.5. Bioinformatic analyses of clinical data revealed FPR1 expression in breast cancer

Before investigating LcrV effects on cancer, we first explored the role of LcrV receptor FPR1 in cancer. Bioinformatics analyses of clinical data were performed to gain insights into FPR1 expression levels and the associations with clinical outcomes. Pan-cancer clinical data showed that FPR1 expression levels varied by tissue type, with FPR1 significantly upregulated in various cancers (Fig. 5A). Among those cancers, breast cancer (BRCA) was the most prevalent worldwide[40]. Furthermore, a growing body of research indicated that FPR1 played a significant role in the progression of breast cancer[16–18,41]. Therefore, we chose breast cancer as a model to investigate the roles of FPR1 in tumor biology. Survival plots further supported the clinical relevance of FPR1, showing that higher expression levels were associated with decreased overall survival and recurrence-free survival in breast cancer patients, with log-rank P values of 0.025 and 0.024, respectively (Fig. 5B). Furthermore, when specifically focusing on breast cancer subtypes, differences in FPR1 expression were found between normal tissues and various breast cancer subtypes, including a significant difference in TNBC. This indicates that FPR1 is more highly expressed in TNBC, which is generally associated with a poorer prognosis (Fig. 5C). These comprehensive bioinformatics analyses suggest a link between elevated FPR1 and aggressive cancer phenotypes and highlight FPR1 as a promising biomarker and therapeutic target in breast cancer.

In the Human Protein Atlas database, the MDA-MB-231 cell line exhibited the highest FPR1 expression (nTPM) among breast cancer cell lines ($n = 62$) based on cell line data from the DepMap portal. Therefore, MDA-MB-231, being the most commonly used TNBC cell line model, was chosen as the cell model for TNBC in this research. Functional FPR1 expression in MDA-MB-231 cells was confirmed by fMLF-stimulated FPR1 responses. The FPR1-specific agonist fMLF stimulated calcium responses in MDA-MB-231 cells, which were inhibited by the

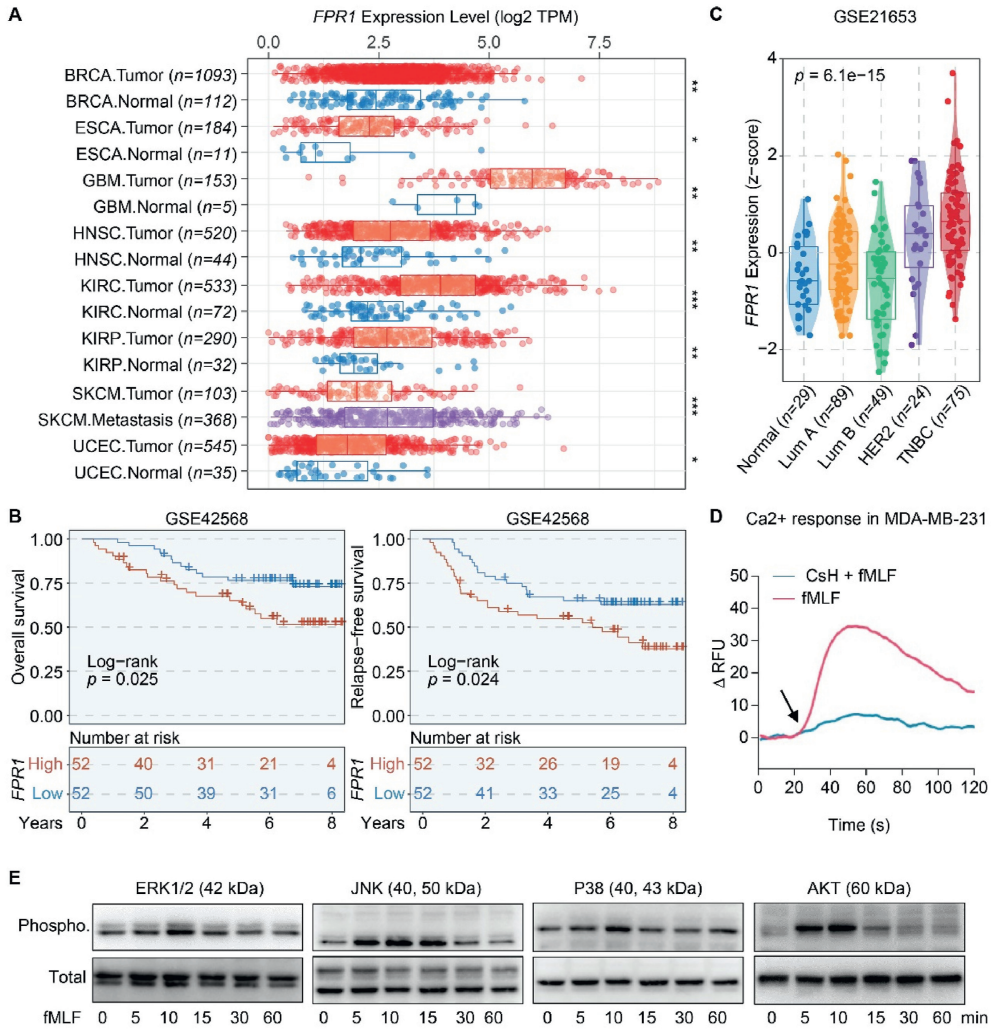

Figure 5 FPR1 expression and its clinical significance in breast cancer. (A) The significant differential expression of FPR1 between tumor and adjacent normal tissues across TCGA tumors is displayed using box plots. BRCA indicates breast cancer. TPM denotes transcripts per million. The Wilcoxon test (*$P < 0.05$; **$P < 0.01$; ***$P < 0.001$) was used to calculate statistical significance. (B) Survival plots of FPR1 expression in relation to overall survival and relapse-free survival, based on the analysis of 104 breast cancer biopsies (GEO: GSE42568). (C) FPR1 expression in breast cancer subtypes (GEO: GSE21653). Lum denotes luminal. (D) FPR1-mediated calcium responses in cancer cells. The calcium response was stimulated by 100 nmol/L fMLF in MDA-MB-231 cells as indicated by the arrow. This response was inhibited by the FPR1 antagonist, 20 μmol/L cyclosporine H. Representative curves are shown. (E) fMLF-stimulated MAPK and PI3K/Akt signaling. MDA-MB-231 cells were treated with 1 μmol/L fMLF for the specified durations. Total and phosphorylated kinases were analyzed by immunoblotting. Representative blots from at least three independent experiments are shown.

FPR1 antagonist cyclosporine H (Fig. 5D). The agonist fMLF also stimulated MAPK and PI3K/Akt signaling pathways in the TNBC cells (Fig. 5E and Supporting Information Fig. S3A).

3.6. Bi-directional modulation of intracellular signaling pathways contributed to the inhibition of TNBC cell proliferation

In MDA-MB-231 cells expressing endogenous FPR1, the biased agonist LcrV was also found to selectively increase JNK and p38 activities while reducing ERK1/2 and Akt phosphorylation (Fig. 6A and Fig. S3B). Quantification analyses confirmed that the full agonist fMLF activated all the MAPK and PI3K/Akt signaling pathways, while the biased agonist LcrV selectively modulated the signaling pathways, similar to the bi-directional modulation observed in the heterologous expression system (Figs. 4C and 6B). Furthermore, G proteins in the cancer cells were inhibited by pertussis toxin (PTX), a specific inhibitor of the Gαi protein, to investigate whether LcrV-stimulated modulation of intracellular kinases was caused by FPR1-G protein signaling transduction. LcrV-stimulated bi-directional modulation of the kinases was generally disrupted by the G protein inhibitor (Fig. 6C and Supporting Information Fig. S4A). Interestingly, LcrV-stimulated p38 activation appeared to be only slightly affected by the inhibitor, suggesting that it may be mediated not only by G proteins but also by β-arrestin2. To further investigate this, we co-treated cancer cells with a specific siRNA designed to knock down β-arrestin2 expression along with PTX. Under this condition, LcrV-stimulated p38 activation was significantly impacted (Fig. 7A and B, Fig. S4B). The p38 activation was not completely inhibited possibly due to residual β-arrestin2 following siRNA knockdown. These findings suggest that, in the cancer cells, the LcrV protein also acts as a biased agonist of FPR1 and stimulates

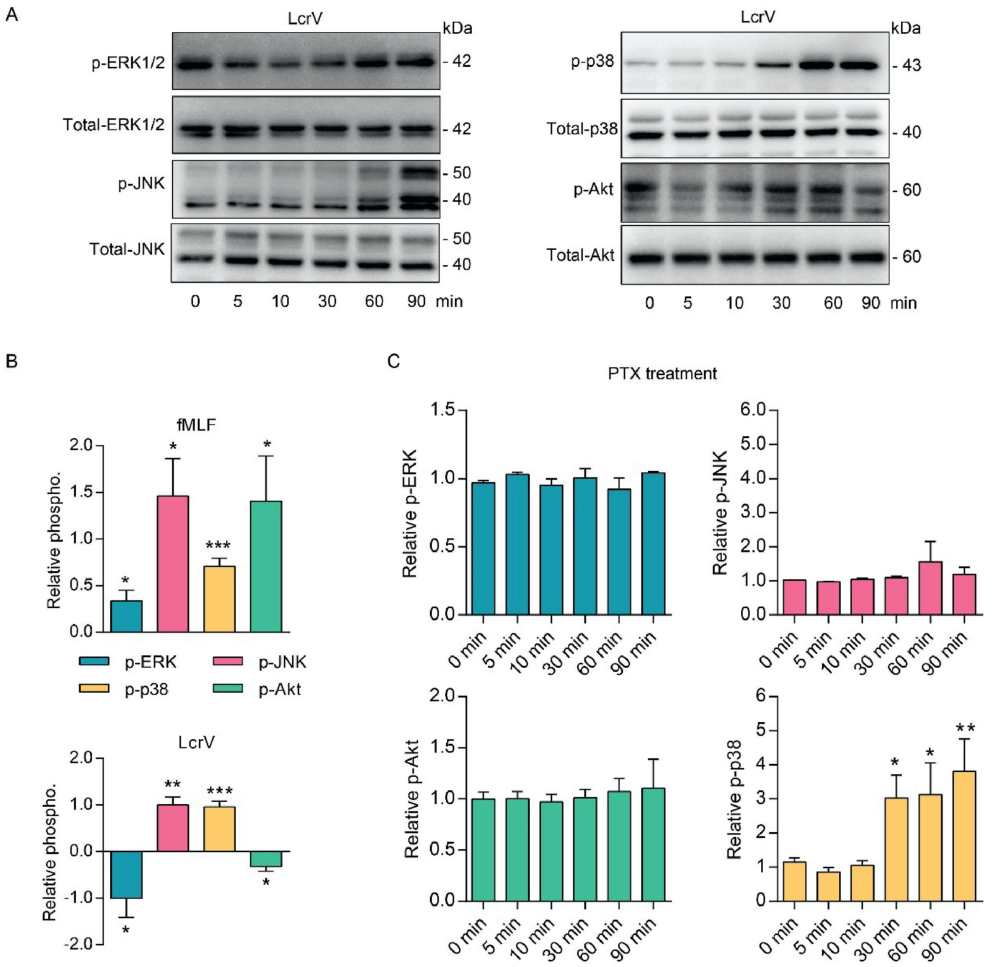

Figure 6 LcrV-stimulated intracellular signaling pathways in TNBC cancer cells. (A) Bi-directional modulation of MAPK and PI3K/Akt signaling. MDA-MB-231 cells were stimulated with 2 μmol/L LcrV. Total and phosphorylated MAPK and Akt were analyzed by immunoblotting. Representative blots are shown ($n = 3-4$). (B) Quantification of phosphorylated protein levels. Data were analyzed as in Figure 4C. For LcrV stimulation, the responses were normalized to the maximum in each direction. (C) The influences of the G protein on LcrV-stimulated signaling. MDA-MB-231 cells were pretreated with 100 ng/mL PTX for at least 6 h. The cells were then stimulated with LcrV, and total and phosphorylated kinases were detected as above. Relative levels of phosphorylated proteins were quantified. Data are presented as mean ± SEM from at least three independent experiments. $^{*}P < 0.05$, $^{**}P < 0.01$, and $^{***}P < 0.001$.

the unconventional G protein activation state, as well as β-arrestin2 recruitment, leading to bi-directional modulation of the intracellular signaling pathways. Given that the MAPK and PI3K/Akt signaling pathways play central roles in orchestrating cell proliferation, it is reasonable to speculate that LcrV could impact cancer cell proliferation.

The impact of LcrV on cancer cell proliferation was investigated by conducting MTT assays. The results revealed that treatment with LcrV for 48 h led to a concentration-dependent decrease in the viabilities of MDA-MB-231 cells (Fig. 7C). Additionally, in MDA-MB-468 cells, another TNBC cell model, LcrV was also found to inhibit cell proliferation. Further analysis using flow cytometry demonstrated that LcrV could impede cell cycle progression within the same time frame. Specifically, LcrV arrested MDA-MB-231 cells in the G1 and S phases of the cell cycle (Fig. 7D). This observation provides insight into how the LcrV protein exerts its inhibitory effects on cancer cell proliferation. FPR1 antagonists have been previously documented to impact cancer progression[18,19]. FPR1 antagonists block all the MAPK and PI3K/Akt signaling pathways downstream of FPR1. However, the biased agonist LcrV bi-directionally modulated FPR1-mediated signaling pathways (Fig. 6B). A comparison between LcrV and the FPR1 antagonist cyclosporine H revealed that LcrV exerted stronger inhibitory effects on cell cycle arrest in cancer cells (Fig. 7D).

To further elucidate the mechanisms underlying the effects of LcrV on tumor cells, cell proliferation was assessed in the presence of ERK1/2 or JNK inhibitors. The results showed that inhibition of ERK1/2 signaling further enhanced the inhibitory effects of LcrV, whereas inhibition of JNK signaling compromised the inhibitory effects (Fig. 7E). In cell cycle analyses, the JNK inhibitor attenuated LcrV-induced cell cycle arrest and the ERK1/2 inhibitor had a tendency to further enhance the cell cycle arrest (Supporting Information Fig. S5). These results indicated that, in the context of LcrV stimulation, ERK1/2 signaling promotes tumor growth while JNK signaling inhibits it. These findings suggest that the biased agonist LcrV exerts anti-tumor effects through dual mechanisms, including increasing tumor-inhibiting signaling and reducing tumor-promoting signaling, which is not observed with conventional FPR1 antagonists.

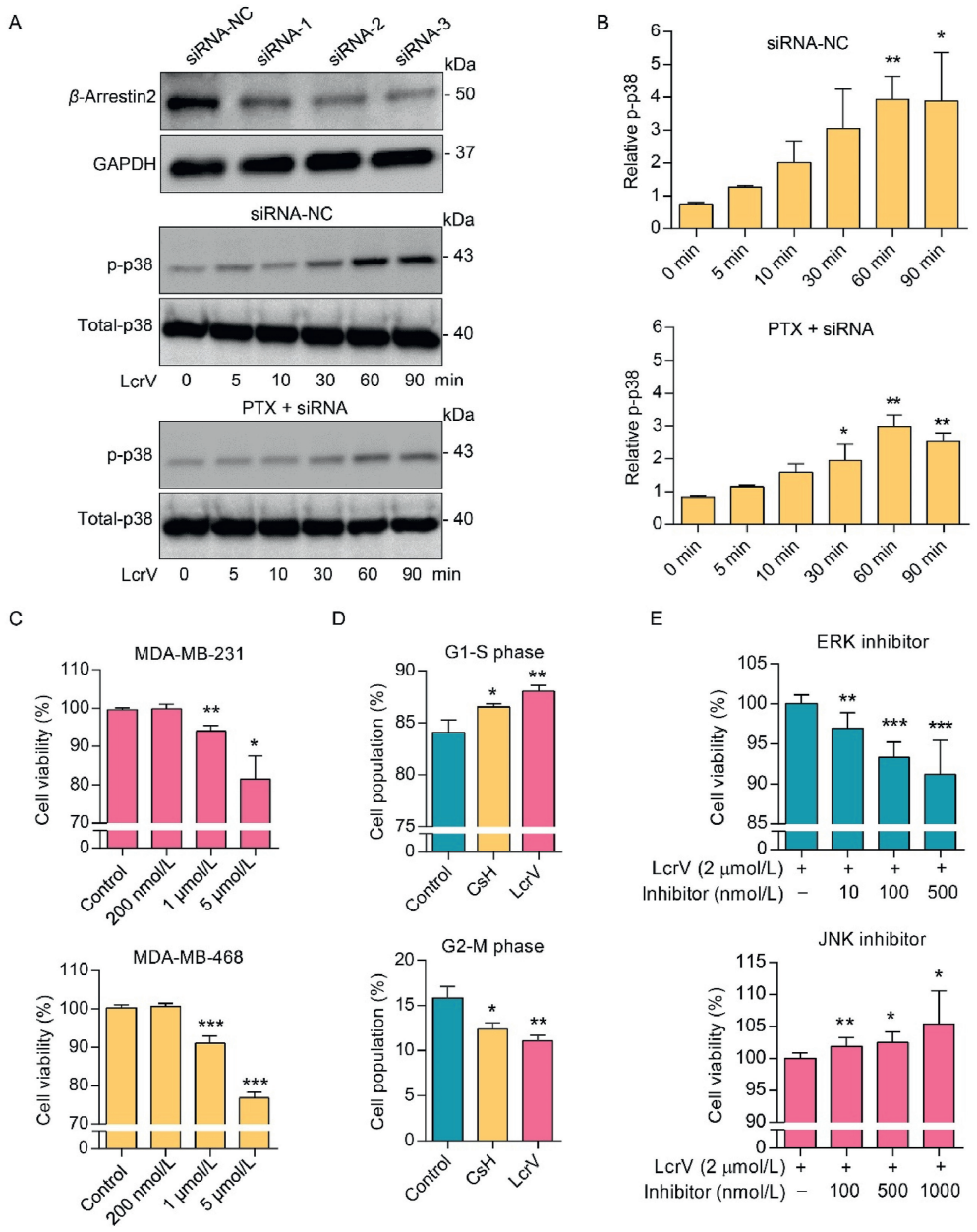

Figure 7 Dual inhibition of G protein and β-arrestin2 and the anti-tumor effects of LcrV. (A) The role of G protein and β-arrestin2 in p38 activation. β-arrestin2 knockdown in MDA-MB-231 cells was confirmed by immunoblotting. MDA-MB-231 cells were pretreated with the control siRNA (siRNA-NC) or siRNA-2 plus PTX. LcrV-stimulated p38 activation was subsequently assessed. Representative blots from at least three independent experiments are shown. (B) Quantification of p38 activation after co-inhibition of G proteins and β-arrestin2. The relative phosphorylation levels were quantified from at least three independent experiments. (C) Effects of LcrV on cell viability. MDA-MB-231 and MDA-MB-468 cells were treated with the indicated concentrations of LcrV for 48 h, and cell viability was analyzed using the MTT assay. (D) Cell cycle arrest induced by FPR1 ligands. MDA-MB-231 cells were stimulated with 2 μmol/L LcrV or 20 μmol/L cyclosporine H. The cells were stained with PI, and the percentages at different cell cycle phases were analyzed using a flow cytometer. (E) Influences of MAPK inhibitors on LcrV actions. MDA-MB-231 cells were treated with 2 μmol/L LcrV plus the indicated concentrations of the ERK1/2 inhibitor SCH772984 or the JNK inhibitor SP600125. Data are shown as mean ± SEM ($n = 3-4$). *$P < 0.05$, **$P < 0.01$, and ***$P < 0.001$.

3.7. LcrV exhibited overwhelming anti-tumor effects over the FPR1 antagonist in vivo

In xenografted breast cancer models established with MDA-MB-231 cells, *in vivo* anti-tumor effects with long-term LcrV treatment were validated. To compare pharmacological effects, the biased agonist LcrV and the FPR1 antagonist cyclosporine H were administered *via* intratumoral injections at doses determined to elicit maximal effects based on *in vitro* assays (Fig. 2E and Supporting Information Fig. S6A). Tumors treated with LcrV showed significantly inhibited growth compared to both mock-treated tumors and those treated with the FPR1 antagonist cyclosporine H (Fig. 8A). Specifically, mock-treated tumors increased in size from approximately 50 to 700 mm^3 after 24 days.

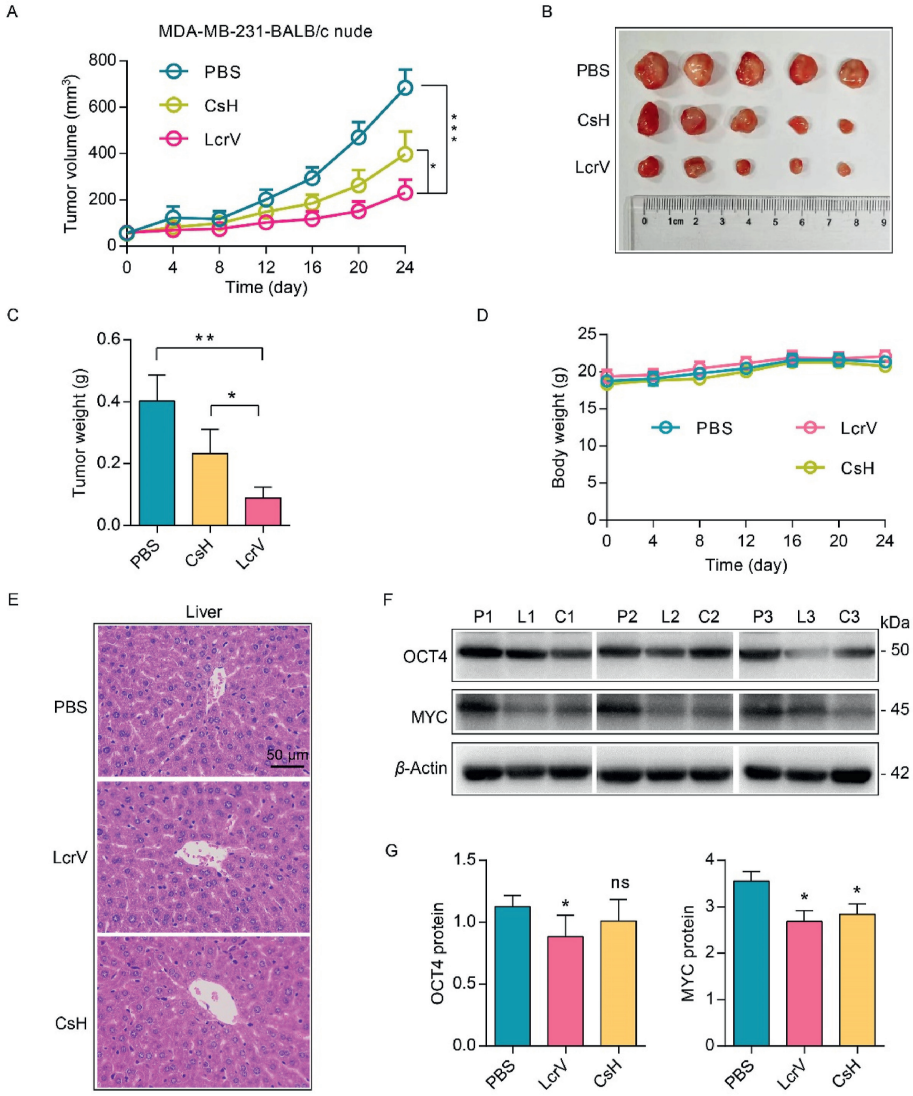

Figure 8 Antitumor activities of LcrV in mouse xenograft models. (A) Kinetics of tumor growth in xenografted mice. BALB/c nude mice implanted with MDA-MB-231 cells received treatments of LcrV, cyclosporine H, or PBS, with tumor dimensions recorded at four-day intervals ($n = 5$). (B) Visual comparison of excised tumors post-treatment. (C) Comparative analysis of tumor mass. Tumor weights were obtained from quintuplicate samples per treatment group and are depicted as mean ± SEM. (D) Body weights of xenografted mice with LcrV treatment. No significant difference was found between different groups ($n = 5$). (E) Histopathological examination of liver tissues. Liver specimens were collected from mice and stained with hematoxylin and eosin. Representative images of at least three sections are shown. Scale bar = 50 μm. (F) Analysis of stemness-associated protein expression in tumors. Immunoblotting was employed to assess OCT4 and MYC levels in MDA-MB-231-derived tumors. The figure shows representative blots for each treatment: PBS (P), LcrV (L), and cyclosporine H (C). (G) Quantification of OCT4 and MYC protein expression. The OCT4 and MYC protein levels were quantified and normalized to the β-actin protein levels ($n = 5$). *$P < 0.05$, **$P < 0.01$, ***$P < 0.001$, and ns indicates no significance.

In contrast, tumors treated with LcrV reached about 200 mm^3 during the same period, even smaller than the 400 mm^3 volume observed in cyclosporine H-treated tumors (Fig. 8A). These superior anti-tumor effects were visually evident in tumor images and were further confirmed by the reduced tumor weights after removal from the mice at the end of the study (Fig. 8B and C).

The anti-tumor effects of LcrV were additionally investigated in a mouse model utilizing 4T1 breast cancer cell lines, where once again LcrV demonstrated greater inhibition of tumor volumes compared to the FPR1 antagonist (Fig. S6B). Since the LcrV protein is a component of the *Yersinia pestis* type III secretion system, the toxicity of the LcrV protein was analyzed in the MDA-MB-231-transplanted mice. Importantly, LcrV treatment did not negatively impact the overall body weight of the mice or affect their liver or lung tissues (Fig. 8D and E, Fig. S6C). This indicates that the observed inhibitory effects on tumor growth were not due to cellular toxicity. These findings underscore the potential of LcrV as an effective and safe anti-tumor agent.

In addition to the observed mechanism of cell cycle arrest in the *in vitro* assays, other potential mechanisms for the anti-tumor effects of the LcrV protein were investigated. The MAPK and PI3K/Akt signaling have many relationships with cancer stemness [42,43]. This suggested LcrV-stimulated signaling might have some impacts on TNBC stemness proteins. In the xenografted model,

mock-treated tumors showed enrichment of c-MYC and OCT4 proteins, whereas tumors treated with LcrV displayed reduced levels of these stemness-associated proteins (Fig. 8F and G). Additionally, the FPR1 antagonist cyclosporine H demonstrated a smaller reduction in stemness proteins overall. The protein levels of SOX2 and beta-catenin were also reduced following LcrV treatment, albeit the reduction was less significant (Fig. S6D). Furthermore, in *in vitro* limited dilution analysis, LcrV treatment was found to inhibit the self-renewal abilities of MDA-MB-231 cells (Supporting Information Table S2). These results indicate that LcrV-stimulated FPR1 signaling has some impacts on tumor stemness-associated phenotypes.

4. Discussion

Targeted therapies based on the HER2 receptor or hormone receptors have made great success in most cases of breast cancer but not in triple-negative breast cancer[44]. It is known that GPCRs mediate critical cell proliferation signals in cancers, including TNBC[2,45]. GPCRs are similar to HER-2 and hormone receptors in various ways, as all these receptors receive extracellular signals and transduce them into the nucleus to promote tumor growth[46,47]. GPCR uses G protein, while HER2 uses Ras protein to stimulate MAPK/ERK and PI3K/Akt signaling pathways, and both G protein and Ras protein belong to the GTPase superfamily. Moreover, GPCR can stimulate epidermal growth factor receptor activation, and conversely, epidermal growth factor receptor can also activate the downstream G proteins of GPCRs, indicating the crosstalk between these two types of receptors[48−50]. Hormone receptors transmit growth signals differently by receptor binding to the genome. However, the isoform of estrogen receptor, GPR30, transduces hormone signaling through G proteins, suggesting intertwined relationships between GPCRs and hormone receptors[51].

Conventional anti-tumor strategies targeting GPCRs mainly involve the use of either agonists or antagonists[3,52,53]. The traditional ligands indiscriminately modulate all the downstream signaling pathways mediated by the receptors. However, GPCRs orchestrate a multitude of cellular processes by engaging diverse signaling pathways. For tumor growth, it is important to recognize that a GPCR can mediate contrast signals, including both promoting and inhibitory signals. Therefore, for cancer treatment, it is not the most effective strategy to use agonists or antagonists to promote or inhibit all GPCR-mediated signaling pathways synchronously. As GPCR research progresses, it is exciting to observe that biased GPCR ligands are being proposed for cancer therapy[54]. A biased ligand of the G protein-coupled bile acid receptor has been reported to activate G proteins, which in turn inhibit the YAP signaling pathway, subsequently reducing cancer cell proliferation[55].

In this research, we presented a biased FPR1 ligand that displayed a unique property of selectively modulating intracellular signaling pathways. The MAPK and PI3K/Akt pathways downstream of FPR1 activation exerted contrasting roles in cancer cell proliferation. ERK1/2 and PI3K/Akt signaling are primarily associated with promoting cancer cell proliferation, whereas JNK and p38 signaling have been reported to inhibit cancer cell proliferation in certain contexts[11,56−58]. In our experimental conditions, it appears that JNK signaling inhibits cell proliferation (Fig. 7E and Fig. S5). Therefore, the biased agonist LcrV was found to decrease the tumor-promoting ERK1/2 and PI3K/Akt signaling while increasing the tumor-inhibiting JNK and p38 signaling (Fig. 9). This bi-directional modulation of signaling pathways was not observed with conventional GPCR agonists or antagonists (Fig. 9). Furthermore, the

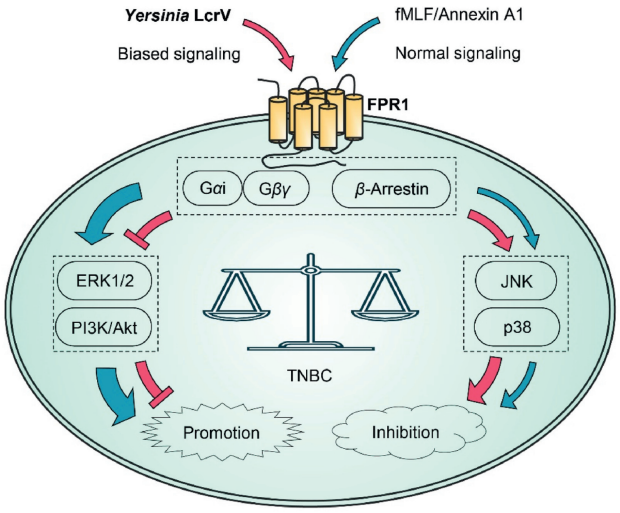

Figure 9 Proposed mechanisms for the anti-tumor effects of biased FPR1 agonist LcrV. TNBC cell proliferation is balanced by both tumor-promoting (*e.g.*, ERK1/2) and tumor-inhibiting (*e.g.*, JNK) signaling pathways. Formyl peptides or annexin A1 activate FPR1, stimulating MAPK and PI3K/Akt signaling through full activation of G proteins and β-arrestins. In this scenario, tumor-promoting signaling predominates, leading to increased cell proliferation. *Yersinia pestis* LcrV, however, induces distinct conformational changes in FPR1, resulting in a specific activation state of G protein. Consequently, LcrV inhibits tumor growth by: 1) stimulating tumor-inhibiting signaling, and 2) inhibiting tumor-promoting signaling. The biased signaling pathway triggered by LcrV is highlighted in red, and conventional agonist-stimulated signaling is shown in blue.

biased ligand LcrV stimulated β-arrestin2 recruitment and FPR1 internalization, which could reduce the amount of cell surface receptors for transducing growth signals[59,60]. Moreover, since LcrV is a large protein that binds to FPR1, it is conceivable that this ligand might hinder the binding of other ligands to the same receptor. Therefore, the biased ligand LcrV exerted anti-tumor effects through the above potential mechanisms.

The LcrV protein used in this study is a component of the type III secretion system of *Yersinia pestis*. Despite *Yersinia pestis* being the causative agent of the plague, the LcrV protein merely functions as a linker or director, enabling the pathogen to attach to human cells[27,28]. The LcrV protein has been administrated to mice in a colitis animal model, indicating its safety for *in vivo* experiments[61]. More commonly, LcrV has been explored for its potential as a component of vaccines, aiming to educate host immune system for the prevention of plague[25,62,63]. This suggests that LcrV may also influence immune cells within the tumor immune microenvironment, warranting further investigation to confirm this potential effect. In the previous study, LcrV was identified as a binding protein of FPR1, and no FPR1-related signaling was reported[28]. We found that the interaction between LcrV and FPR1 led to a unique conformational change of the receptor, as demonstrated by an intramolecular BRET biosensor. Subsequent investigations revealed that LcrV protein stimulated G protein and β-arrestin protein in a biased manner. Interestingly, the G protein complex did not dissociate, and calcium mobilization was not detected, while GRK3 could still associate with the G$\beta\gamma$ subunits and cAMP responses were detected. This might be caused by the noncanonical rearrangement of the G protein subunits, as

described in other circumstances[64]. It has been reported that one G protein can transduce at least two types of extracellular signals and stimulate distinct intracellular signaling pathways, each playing different roles in tumor growth[65]. The specific activation state of the G protein may explain why LcrV can bi-directionally modulate the MAPK and PI3K/Akt signaling pathways, thereby inhibiting tumor growth.

As far as we know, the biased signaling behavior of LcrV has not been reported for other FPR1 ligands. This indicated that the anti-tumor actions might be the unique property of the LcrV protein and not shared by other FPR1 ligands. The elaborate modulation of MAPK and PI3K/Akt signaling pathways might not explain all the molecular mechanisms. Further investigations on the entire intracellular signaling networks will be required to unravel additional mechanisms. Moreover, it remains an open question how LcrV binds to FPR1. At present, no cryo-EM or crystallization data of LcrV-FPR1 complex are available to answer this question. We have prepared both N-terminally tagged and C-terminally tagged LcrV proteins, and no differences in the anti-tumor efficacy were found between them. This suggests that the N-terminal of the LcrV protein may not be inserted into the canonical binding pocket of FPR1, as the previous study predicated[28]. Direct evidence from a cryo-EM or crystallization structure is needed to obtain more information for ligand optimization and drug development.

5. Conclusions

The anti-tumor effects of *Yersinia* LcrV protein have highlighted the potential of biased GPCR ligands in cancer therapy. Understanding the molecular mechanisms of this biased ligand is expected to facilitate the development of many other biased ligands targeting a wide range of GPCRs. The biased signaling repertoire of the LcrV protein may not be the most effective for cancer therapy. Further investigations based on our study are likely to lead to the discovery of more effective biased ligands, capable of precisely regulating tumor-promoting and tumor-inhibiting signaling pathways for cancer treatment.

Acknowledgments

This work was supported by National Natural Science Foundation of China (Nos. 82202910 and 81603158), Jiangnan University Medical Discipline Development Funds (Nos. YXXK2024092612 and YXXK2024092602, China), Yunnan Key Research and Development Program Grant (No. 202402AA310032, R.D.Y., China), Shenzhen Medical Research Fund (No. SMRF-D2403009, R.D.Y., China), and the Fundamental Research Funds for the Central Universities (No. JUSRP123072, China). We extend our gratitude to Ms. Fan Yu at Wuxi School of Medicine, Jiangnan University, for technical assistance.

Author contributions

Yunjun Ge: Writing − review & editing, Writing − original draft, Project administration, Investigation, Funding acquisition, Formal analysis, Conceptualization. Huiwen Guan: Investigation, Data curation. Ting Li: Software, Formal analysis. Jie Wang: Investigation, Formal analysis. Liang Ying: Investigation. Shuhui Guo: Writing − review & editing, Visualization. Jinjian Lu: Writing − review & editing. Richard D. Ye: Writing − review & editing, Supervision, Resources, Funding acquisition, Conceptualization. Guosheng Wu: Writing − review & editing, Supervision, Resources, Methodology, Funding acquisition, Formal analysis, Conceptualization.

Conflicts of interest

The authors declare no conflicts of interest.

Appendix A. Supporting information

Supporting information to this article can be found online at https://doi.org/10.1016/j.apsb.2025.04.030.

References

1. Hauser AS, Attwood MM, Rask-Andersen M, Schioth HB, Gloriam DE. Trends in GPCR drug discovery: new agents, targets and indications. *Nat Rev Drug Discov* 2017;**16**:829−42.
2. Dorsam RT, Gutkind JS. G-protein-coupled receptors and cancer. *Nat Rev Cancer* 2007;**7**:79−94.
3. Lappano R, Maggiolini M. G protein-coupled receptors: novel targets for drug discovery in cancer. *Nat Rev Drug Discov* 2010;**10**:47−60.
4. Tan L, Yan W, McCorvy JD, Cheng J. Biased Ligands of G Protein-coupled receptors (GPCRs): structure−functional selectivity relationships (SFSRs) and therapeutic potential. *J Med Chem* 2018;**61**: 9841−78.
5. Slosky LM, Caron MG, Barak LS. Biased allosteric modulators: new frontiers in GPCR drug discovery. *Trends Pharmacol Sci* 2021;**42**: 283−99.
6. Crudden C, Shibano T, Song D, Dragomir MP, Cismas S, Serly J, et al. Inhibition of G protein-coupled receptor kinase 2 promotes unbiased downregulation of IGF1 receptor and restrains malignant cell growth. *Cancer Res* 2021;**81**:501−14.
7. Bresnick AR, Backer JM. PI3Kβ—a versatile transducer for GPCR, RTK, and small GTPase signaling. *Endocrinology* 2019;**160**:536−55.
8. Cheng Z, Li JF, Niu Y, Zhang XC, Woody OZ, Xiong Y, et al. Pathogen-secreted proteases activate a novel plant immune pathway. *Nature* 2015;**521**:213−6.
9. Chen XL, Zhang JB, Xia L, Wang L, Li H, Liu HL, et al. β-Arrestin-2 attenuates hepatic ischemia-reperfusion injury by activating PI3K/Akt signaling. *Aging-Us* 2021;**13**:2251−63.
10. Zhang W, Liu HT. MAPK signal pathways in the regulation of cell proliferation in mammalian cells. *Cell Res* 2002;**12**:9−18.
11. Pereira SS, Monteiro MP, Costa MM, Ferreira J, Alves MG, Oliveira PF, et al. MAPK/ERK pathway inhibition is a promising treatment target for adrenocortical tumors. *J Cell Biochem* 2019;**120**: 894−906.
12. Canovas B, Nebreda AR. Diversity and versatility of p38 kinase signalling in health and disease. *Nat Rev Mol Cell Biol* 2021;**22**:346−66.
13. Wagner EF, Nebreda ÁR. Signal integration by JNK and p38 MAPK pathways in cancer development. *Nat Rev Cancer* 2009;**9**:537−49.
14. He Y, Sun MM, Zhang GG, Yang J, Chen KS, Xu WW, et al. Targeting PI3K/Akt signal transduction for cancer therapy. *Signal Transduct Target Ther* 2021;**6**:425.
15. Cao G, Zhang Z. FPR1 mediates the tumorigenicity of human cervical cancer cells. *Cancer Manag Res* 2018;**10**:5855−65.
16. Khau T, Langenbach SY, Schuliga M, Harris T, Johnstone CN, Anderson RL, et al. Annexin-1 signals mitogen-stimulated breast tumor cell proliferation by activation of the formyl peptide receptors (FPRs) 1 and 2. *FASEB J* 2011;**25**:483−96.
17. Al-Ali HN, Crichton SJ, Fabian C, Pepper C, Butcher DR, Dempsey FC, et al. A therapeutic antibody targeting annexin-A1 inhibits cancer cell growth *in vitro* and *in vivo*. *Oncogene* 2024;**43**: 608−14.

18. Vecchi L, Alves Pereira Zoia M, Goss Santos T, de Oliveira Beserra A, Colaco Ramos CM, Franca Matias Colombo B, et al. Inhibition of the AnxA1/FPR1 autocrine axis reduces MDA-MB-231 breast cancer cell growth and aggressiveness *in vitro* and *in vivo*. *Biochim Biophys Acta Mol Cell Res* 2018;**1865**:1368−82.
19. Ahmet DS, Basheer HA, Salem A, Lu D, Aghamohammadi A, Weyerhauser P, et al. Application of small molecule FPR1 antagonists in the treatment of cancers. *Sci Rep* 2020;**10**:17249.
20. Ye RD, Boulay F, Wang JM, Dahlgren C, Gerard C, Parmentier M, et al. International union of basic and clinical pharmacology. LXXIII. Nomenclature for the formyl peptide receptor (FPR) family. *Pharmacol Rev* 2009;**61**:119−61.
21. He HQ, Ye RD. The formyl peptide receptors: diversity of ligands and mechanism for recognition. *Molecules* 2017;**22**:455.
22. Saito N, Qiao H, Yanagi T, Shinkuma S, Nishimura K, Suto A, et al. An annexin A1-FPR1 interaction contributes to necroptosis of keratinocytes in severe cutaneous adverse drug reactions. *Sci Transl Med* 2014;**6**:245ra95.
23. Zhang S, Gong H, Ge Y, Ye RD. Biased allosteric modulation of formyl peptide receptor 2 leads to distinct receptor conformational states for pro- and anti-inflammatory signaling. *Pharmacol Res* 2020; **161**:105117.
24. Ge Y, Zhang S, Wang J, Xia F, Wan JB, Lu J, et al. Dual modulation of formyl peptide receptor 2 by aspirin-triggered lipoxin contributes to its anti-inflammatory activity. *FASEB J* 2020;**34**:6920−33.
25. Demeure CE, Dussurget O, Mas Fiol G, Le Guern AS, Savin C, Pizarro-Cerda J. Yersinia pestis and plague: an updated view on evolution, virulence determinants, immune subversion, vaccination, and diagnostics. *Gene Immun* 2019;**20**:357−70.
26. Mitchell A, Tam C, Elli D, Charlton T, Osei-Owusu P, Fazlollahi F, et al. Glutathionylation of *Yersinia pestis* LcrV and its effects on plague pathogenesis. *mBio* 2017;**8**:e00646-17.
27. Mueller CA, Broz P, Muller SA, Ringler P, Erne-Brand F, Sorg I, et al. The V-antigen of Yersinia forms a distinct structure at the tip of injectisome needles. *Science* 2005;**310**:674−6.
28. Osei-Owusu P, Charlton TM, Kim HK, Missiakas D, Schneewind O. FPR1 is the plague receptor on host immune cells. *Nature* 2019;**574**: 57−62.
29. Depaolo RW, Tang F, Kim I, Han M, Levin N, Ciletti N, et al. Toll-like receptor 6 drives differentiation of tolerogenic dendritic cells and contributes to LcrV-mediated plague pathogenesis. *Cell Host Microbe* 2008;**4**:350−61.
30. Overheim KA, DePaolo RW, DeBord KL, Morrin EM, Anderson DM, Green NM, et al. LcrV plague vaccine with altered immunomodulatory properties. *Infect Immun* 2005;**73**:5152−9.
31. Wang J, Ye RD. Agonist concentration-dependent changes in FPR1 conformation lead to biased signaling for selective activation of phagocyte functions. *Proc Natl Acad Sci U S A* 2022;**119**: e2201249119.
32. Inoue A, Raimondi F, Kadji FMN, Singh G, Kishi T, Uwamizu A, et al. Illuminating G-protein-coupling selectivity of GPCRs. *Cell* 2019;**177**:1933−47.e25.
33. Wang J, Chen G, Liao Q, Lyu W, Liu A, Zhu L, et al. Cryo-EM structure of the human chemerin receptor 1-Gi protein complex bound to the C-terminal nonapeptide of chemerin. *Proc Natl Acad Sci U S A* 2023;**120**:e2214324120.
34. Maziarz M, Park JC, Leyme A, Marivin A, Garcia-Lopez A, Patel PP, et al. Revealing the activity of trimeric G-proteins in live cells with a versatile biosensor design. *Cell* 2020;**182**:770−85.e16.
35. Li T, Fu J, Zeng Z, Cohen D, Li J, Chen Q, et al. TIMER2.0 for analysis of tumor-infiltrating immune cells. *Nucleic Acids Res* 2020; **48**. W509-w14.
36. Liu Z, Liu L, Weng S, Xu H, Xing Z, Ren Y, et al. BEST: a web application for comprehensive biomarker exploration on large-scale data in solid tumors. *J Big Data* 2023;**10**:165.
37. Hu Y, Smyth GK. ELDA: extreme limiting dilution analysis for comparing depleted and enriched populations in stem cell and other assays. *J Immunol Methods* 2009;**347**:70−8.
38. Stribbling SM, Ryan AJ. The cell-line-derived subcutaneous tumor model in preclinical cancer research. *Nat Protoc* 2022;**17**: 2108−28.
39. Ge YJ, Liao QW, Xu YC, Zhao Q, Wu BL, Ye RD. Anti-inflammatory signaling through G protein-coupled receptors. *Acta Pharmacol Sin* 2020;**41**:1531−8.
40. Loibl S, Poortmans P, Morrow M, Denkert C, Curigliano G. Breast cancer. *Lancet* 2021;**397**:1750−69.
41. Le Naour J, Liu P, Zhao L, Adjemian S, Sztupinszki Z, Taieb J, et al. A TLR3 Ligand reestablishes chemotherapeutic responses in the context of FPR1 deficiency. *Cancer Discov* 2021;**11**:408−23.
42. Schaefer T, Lengerke C. SOX2 protein biochemistry in stemness, reprogramming, and cancer: the PI3K/AKT/SOX2 axis and beyond. *Oncogene* 2019;**39**:278−92.
43. Li LJ, Sun L, Gao FR, Jiang J, Yang Y, Li CL, et al. Stk40 links the pluripotency factor Oct4 to the Erk/MAPK pathway and controls extraembryonic endoderm differentiation. *P Natl Acad Sci USA* 2010; **107**:1402−7.
44. Wang Y, Min J, Deng X, Feng T, Hu H, Guo X, et al. Discovery of novel covalent selective estrogen receptor degraders against endocrine-resistant breast cancer. *Acta Pharm Sin B* 2023;**13**: 4963−82.
45. Lappano R, Maggiolini M. GPCRs and cancer. *Acta Pharmacol Sin* 2012;**33**:351−62.
46. Ekambaram P, Lee JY, Hubel NE, Hu D, Yerneni S, Campbell PG, et al. The CARMA3−Bcl10−MALT1 signalosome drives NFκB activation and promotes aggressiveness in angiotensin II receptor−positive breast cancer. *Cancer Res* 2018;**78**:1225−40.
47. Pawar NR, Buzza MS, Antalis TM. Membrane-anchored serine proteases and protease-activated receptor-2−mediated signaling: co-conspirators in cancer progression. *Cancer Res* 2019;**79**:301−10.
48. Daub H, Weiss FU, Wallasch C, Ullrich A. Role of transactivation of the EGF receptor in signalling by G-protein-coupled receptors. *Nature* 1996;**379**:557−60.
49. Bhola NE, Grandis JR. Crosstalk between G-protein-coupled receptors and Epidermal growth factor receptor in cancer. *Front Biosci-Landmrk* 2008;**13**:1857−65.
50. Garcia-Marcos M, Ghosh P, Farquhar MG. GIV/Girdin transmits signals from multiple receptors by triggering trimeric G protein activation. *J Biol Chem* 2015;**290**:6697−704.
51. Wang ZY, Yin L. Estrogen receptor alpha-36 (ER-α36): a new player in human breast cancer. *Mol Cell Endocrinol* 2015;**418**: 193−206.
52. Le Naour J, Thierry S, Scuderi SA, Boucard-Jourdin M, Liu P, Bonnin M, et al. A chemically defined TLR3 agonist with anticancer activity. *OncoImmunology* 2023;**12**:2227510.
53. Chen L, Xu GY, Song XX, Zhang LB, Chen CY, Xiang G, et al. A novel antagonist of the CCL5/CCR5 axis suppresses the tumor growth and metastasis of triple-negative breast cancer by CCR5-YAP1 regulation. *Cancer Lett* 2024;**583**:216635.
54. Yang F, Mao CY, Guo LL, Lin JY, Ming QQ, Xiao P, et al. Structural basis of GPBAR activation and bile acid recognition. *Nature* 2020; **587**:499−504.
55. Ma L, Yang F, Wu X, Mao C, Guo L, Miao T, et al. Structural basis and molecular mechanism of biased GPBAR signaling in regulating NSCLC cell growth *via* YAP activity. *Proc Natl Acad Sci USA* 2022; **119**:e2117054119.
56. Sui X, Kong N, Ye L, Han W, Zhou J, Zhang Q, et al. p38 and JNK MAPK pathways control the balance of apoptosis and autophagy in response to chemotherapeutic agents. *Cancer Lett* 2014;**344**:174−9.
57. Song Y, Bi Z, Liu Y, Qin F, Wei Y, Wei X. Targeting RAS−RAF−MEK−ERK signaling pathway in human cancer: current status in clinical trials. *Genes Dis* 2023;**10**:76−88.
58. Qin K, Yu S, Liu Y, Guo R, Guo S, Fei J, et al. USP36 stabilizes nucleolar Snail1 to promote ribosome biogenesis and cancer cell survival upon ribotoxic stress. *Nat Commun* 2023; **14**:6473.

59. Kim GT, Kim EY, Shin S-H, Lee H, Lee SH, Sohn K-Y, et al. Suppression of tumor progression by thioredoxin-interacting protein-dependent adenosine 2B receptor degradation in a PLAG-treated Lewis lung carcinoma-1 model of non−small cell lung cancer. *Neoplasia* 2022;**31**:100815.
60. Yu S, Sun L, Jiao Y, Lee LTO. The role of G protein-coupled receptor kinases in cancer. *Int J Biol Sci* 2018;**14**:189−203.
61. Foligne B, Dessein R, Marceau M, Poiret S, Chamaillard M, Pot B, et al. Prevention and treatment of colitis with *Lactococcus lactis* secreting the immunomodulatory Yersinia LcrV protein. *Gastroenterology* 2007;**133**:862−74.
62. Heine SJ, Franco-Mahecha OL, Sears KT, Drachenberg CB, van Roosmalen ML, Leenhouts K, et al. A combined YopB and LcrV subunit vaccine elicits protective immunity against Yersinia infection in adult and infant mice. *J Immunol* 2019;**202**:2005−16.
63. Kilgore PB, Sha J, Hendrix EK, Motin VL, Chopra AK. Combinatorial viral vector-based and live attenuated vaccines without an adjuvant to generate broader immune responses to effectively combat pneumonic plague. *mBio* 2021;**12**:e0322321.
64. Bunemann M, Frank M, Lohse MJ. Gi protein activation in intact cells involves subunit rearrangement rather than dissociation. *Proc Natl Acad Sci USA* 2003;**100**:16077−82.
65. Zhao JY, DiGiacomo V, Ferreras-Gutierrez M, Dastjerdi S, Opakua AID, Park JC, et al. Small-molecule targeting of GPCR-independent noncanonical G-protein signaling in cancer. *P Natl Acad Sci USA* 2023;**120**:e2213140120.